Techniques for Graceful Reversion from Dual to Single Frequency WAAS

Shau-Shiun Jan, Todd Walter, Per Enge
Department of Aeronautics and Astronautics
Stanford University, California 94305

ABSTRACT

This paper investigates techniques to sustain dual-frequency ionosphere performance when a dual-frequency airborne user loses all but one GPS frequency while descending into the radio frequency interference (RFI) field. In this paper, we are particularly interested in the case where the user transitions from L1-L5 to having L5-only. That is because the uncertainty of the L5-only ionospheric delay estimation is larger than the L1-only ionospheric delay estimation.

An L1-L5 dual-frequency user has LPV (HAL = 40m, VAL = 50m) [1] precision approach services available 99.9% of time over 100% CONUS, with a nominal σ_{UIRE} of 0.32m [2]. An L5 single-frequency user has LPV precision approach services available 99.9% of time over 49.25% CONUS [3]. In this situation, the nominal σ_{UIRE} is 6m at coast lines, and 3.5m at the center. In other words, if an L1-L5 dual-frequency user loses L1 GPS frequency due to RFI and instead uses the WAAS grid for ionospheric delay estimation, the loss of CONUS coverage of LPV services will be about 50%. Therefore, the objective of this paper is to find solutions that will sustain a performance similar to the multi-frequency ionospheric delay estimation.

Based on the information available to user, there are three techniques to sustain the dual-frequency ionospheric delay estimation. This paper uses a typical precision approach example based on San Francisco International Airport (SFO) to examine the possible solutions, and then uses the MATLAB Algorithm Availability Simulation Tool (MAAST) [4] to measure all airports over CONUS. First, one can use the code-carrier divergence to continue ionospheric delay estimation; this technique would require a robust cycle slip detector. This technique provides good ionospheric delay estimation (better than using the WAAS [5] grid) for the full duration of approach. Second, one can use the WAAS ionospheric threat model to bound the error. This technique requires an ionosphere storm detector. It provides useful ionospheric delay estimation for at least 10 minutes. Third, one can use the maximum ionospheric delay gradient model to estimate ionospheric delay during the ionosphere storm period. This technique should only be used when there is no available ionosphere storm detector. The maximum ionospheric delay gradient technique also provides useful ionospheric delay estimation for at least 10 minutes.

I. INTRODUCTION

A dual-frequency GPS user can estimate the ionospheric delay directly and then subtract this estimation from the pseudorange measurements. This direct use of the dual-frequency will be more accurate and offer higher availability. [2] showed the simulation results of the CONUS (CONterminous US) coverage of the LPV [1] precision approach services for a dual-frequency user. While experiencing the RFI (Radio Frequency Interference), a dual-frequency user might lose all but one GPS frequency, which introduces the single-frequency GPS user cases. [3] showed the simulation results of the CONUS coverage of the LPV precision approach services for a single-frequency user. While comparing the results of [3] with [2], the CONUS coverage of LPV precision approach services for a single frequency user is less than the coverage for a dual-frequency user. Therefore, the objective of this paper is to investigate techniques which can sustain dual-frequency performance while descending into the RFI field.

This paper discusses the aviation application, as the L1 and L5 GPS frequencies are in ARNS (Aeronautical Radio Navigation Services). We are particularly interested in the case where the user transitions from L1-L5 to having L5-only. That is because the uncertainty of the L5-only ionospheric delay estimation is larger than the L1-only ionospheric delay estimation. This is because ionospheric delay is inversely proportional to frequency and L5 is a lower frequency than L1.

This paper is organized as follows. Section II discusses the problem, scenarios, and proposed techniques. The code and carrier divergence technique will be discussed in Section III. Section IV investigates the WAAS

ionosphere threat model technique. The maximum ionospheric delay gradient model technique is discussed in Section V. Each section will include a typical precision approach example based on San Francisco International Airport, and followed by the MAAST simulation results for all airports within CONUS. Section VI presents a summary and concluding remarks.

II. PROBLEM STATEMENT AND SCENARIOS

An L1-L5 dual-frequency user has LPV (HAL = 40m, VAL = 50m) precision approach services available 99.9% of time over 100% CONUS. The nominal σ_{UIRE} is 0.32m [2]. An L5 single-frequency user has LPV precision approach services available 99.9% of time over 49.25% CONUS [3]. In this situation, the nominal σ_{UIRE} is 6m at the coast, and 3.5m in the center. In other words, if an L1-L5 dual-frequency user lose L1 due to RFI and instead uses the WAAS grid for ionospheric delay estimation, the loss of CONUS coverage of LPV services will be about 50%. The loss of CONUS coverage of LPV services is mainly because of the uncertainty of the ionospheric delay on L5. This situation is summarized in Figure 1. All VPL maps used in this paper are for 99.9% availability, that is, a user at each specific location had a VPL equal to or below the value indicated by the color bar for 99.9% of time.

Consider a typical precision approach example based on the San Francisco International Airport (SFO). In this example, the final approach length is about 14.1 nm (26.1 km), and the final approach velocity for a general aviation (GA) aircraft is 90-120 knots (167-222 km/hour). Thus the final approach duration is about 7-9 minutes depending on the final approach velocity. We assume that the aircraft enters the boundary of the L1 RFI field when the aircraft reaches the final approach fix. This example is shown in Figure 2. Therefore, for this typical precision approach example, a qualified technique must provide at least 9-minute of useful ionospheric delay estimation, similar to performance of the dual-frequency ionospheric delay estimation.

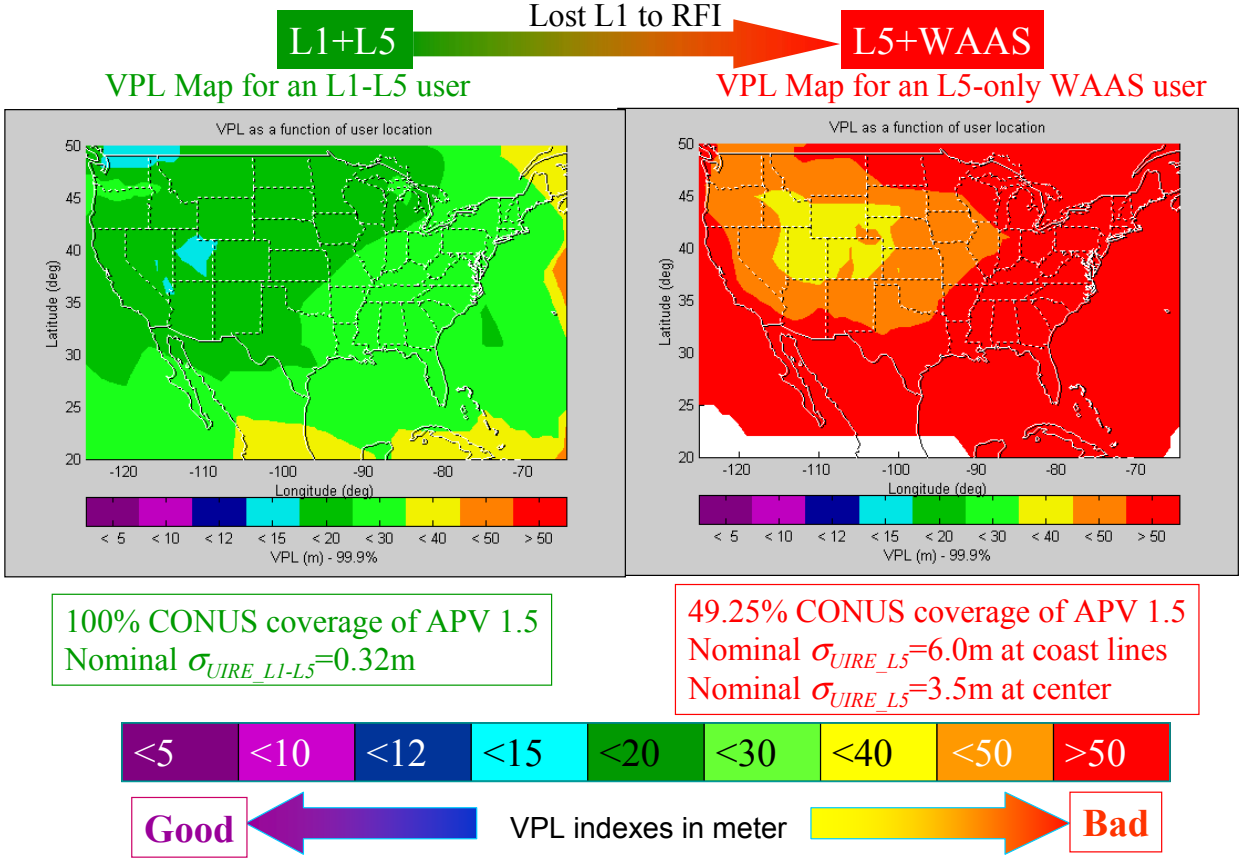

Figure 1: The VPL maps illustrate the situation when an L1-L5 dual-frequency user is descending into an L1 RFI field. The VPL map on the left is for an L1-L5 dual-frequency airborne user right before entering the L1 RFI field. The VPL map on the right is for an L5 single-frequency WAAS user. The loss of CONUS coverage of LPV services will be about 50% for this example. Both plots are 99.9% VPL maps.

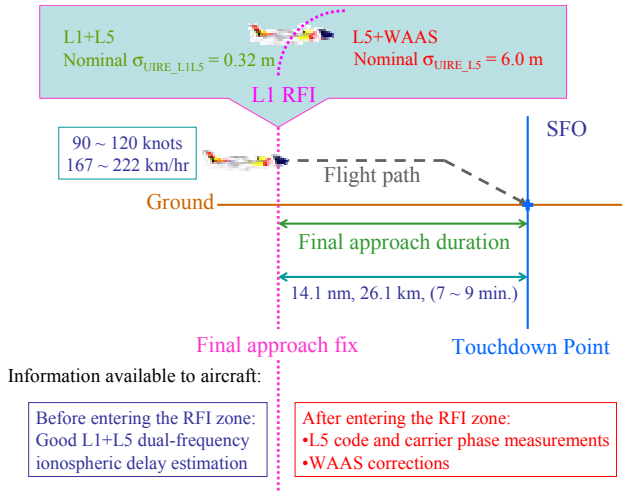

Figure 2: A typical precision approach duration example based on San Francisco International Airport (SFO). The aircraft enters the boundary of the L1 RFI field when the aircraft reaches the final approach fix. The nominal σ_{UIRE} jumps from 0.32m to 6.0m, which results the loss of CONUS coverage of LPV services.

Figure 2 also shows the available information to an aircraft before and after entering the RFI field. Before entering the L1 RFI field, an aircraft has good L1-L5 dual-frequency ionospheric delay estimation. After entering the L1 RFI field, an aircraft has L5 single-frequency code and carrier phase measurements, and WAAS corrections. We explore three techniques to sustain the dual-frequency ionospheric delay estimation.

- L5 code and carrier divergence.
- WAAS ionospheric threat model.
- Maximum ionospheric delay gradient model.

The requirements for these techniques are shown in Figure 3. The requirement for using the L5 code and carrier divergence technique is the absence of cycle slips. When cycle slips are present, and if there is no ionosphere storm, one could utilize the WAAS ionospheric threat model technique. If both cycle slips and ionosphere storm may be present, one could use the maximum ionospheric delay gradient model technique.

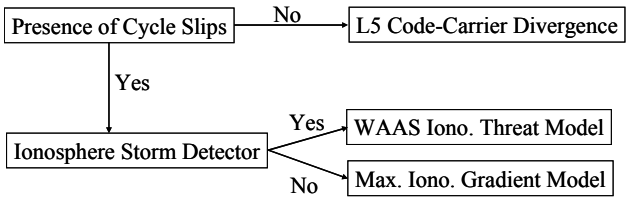

Figure 3: Techniques sustain the performance of the L1-L5 dual-frequency ionospheric delay estimation, and the required conditions for using these techniques.

The 9-minute final approach duration used in this paper was derived from the final approach velocity of the general aviation (GA) aircraft, but these techniques are not limited to the GA aircraft. The final approach velocities of the commercial airliner are faster than the GA aircraft, so the final approach duration is shorter in time.

III. THE CODE AND CARRIER DIVERGENCE TECHNIQUE

The basic observables of a single-frequency receiver include [6]:

$$\rho = R_j^i + b_j - B^i + I_j^i + T_j^i + M_j^i + \nu_j^i \quad (1)$$

$$\phi = R_j^i + b_j - B^i - I_j^i + T_j^i + N_j^i\lambda + m_j^i + \varepsilon_j^i \quad (2)$$

$$\rho - \phi = 2I_j^i + N_j^i\lambda + M_j^i + \nu_j^i - m_j^i - \varepsilon_j^i \quad (3)$$

Where,

R_j^i = true range from SV_i to $user_j$

b_j = receiver offset from UTC

B^i = satellite clock offset from UTC

I = ionospheric delay

T = tropospheric delay

M = multipath delay

ν = receiver thermal noise

$N_j^i\lambda$ = integer ambiguity

One distinction between the code and carrier observables is the magnitude of the multipath and noise terms which are fractions of a wavelength ($\lambda_{L1} \approx 19$ cm, $\lambda_{L2} \approx 24$ cm, $\lambda_{L5} \approx 25$ cm, and $\lambda_\rho \approx 300$ m). For the carrier signal the m_j^i and ε_j^i terms are over two orders of magnitude smaller than the corresponding M_j^i and ν_j^i on the pseudorange observations. At that level they are negligible, and equation (3) can be rewritten as:

$$\rho - \phi = 2I_j^i + N_j^i\lambda + M_j^i + \nu_j^i \quad (4)$$

In equation (4) the ν_j^i term, can be averaged out easily, and the M_j^i term can be mitigated by the aircraft antenna environment. Although the multipath and noise errors could be limited to a reasonably low level, equation (4) still suffers from an integer ambiguity ($N_j^i\lambda$). Fortunately, the integer ambiguity is a constant offset unless there is a cycle slip. As a result, there are two methods to solve the integer ambiguity in equation (4).

First, one can take advantage of the integer ambiguity solution before losing all but one GPS frequency while descending into the RFI field, and then subtract this solution from equation (4). Thus, the ionospheric delay can be calculated as in equation (5-6).

$$\rho - \phi = 2\hat{I}_j^i \tag{5}$$

$$\hat{I}_j^i = \frac{\rho - \phi}{2} \tag{6}$$

Second, one can take advantage of the WAAS ionosphere corrections to solve the integer ambiguity from the information fusion viewpoint [7]. Specifically, user integer ambiguity can be estimated by combining the user local observables and WAAS messages, as shown in equation (7).

$$\frac{N_j^i \lambda}{2} + \xi = \frac{\rho - \phi}{2} + I_{WAAS} \tag{7}$$

Where, ξ is the residual error of the estimation, and I_{WAAS} is the WAAS ionosphere corrections.

Therefore, the ionospheric delay can be estimated by the code and carrier divergence technique, as in equation (8).

$$\hat{I}_{\rho\phi} = \frac{\rho - \phi}{2} - \frac{\hat{N}\lambda}{2} \tag{8}$$

This paper uses the observables of satellite number 20 collected at Stanford University on July 13, 2001 as an example. Figure 4 shows the slant ionospheric delay in meters measured in three methods. The blue line shows the ionospheric delay $I_{L1\rho}$ at the L1 frequency as measured by the L1 and L2 code difference. The equation with which pseudorange measurements ρ_{L1} and ρ_{L2} at the L1 and L2 frequency, respectively, can be used to measure the ionospheric delay $I_{L1\rho}$ at L1 is

$$I_{L1\rho} = \frac{f_{L2}^2}{\left(f_{L1}^2 - f_{L2}^2\right)}\left(\rho_{L2} - \rho_{L1}\right) \tag{9}$$

This measurement of the slant ionospheric delay is noisy but unambiguous.

The red line plots the delay $I_{L1\phi}$ at L1 as obtained from the L1 and L2 carrier phase measurements, ϕ_{L1} and ϕ_{L2}. The equation with which carrier phase measurements ϕ_{L1} and ϕ_{L2} at the L1 and L2 frequency, respectively, can be used to measure the ionospheric delay $I_{L1\phi}$ at L1 is

$$I_{L1\phi} = \frac{f_{L2}^2}{\left(f_{L1}^2 - f_{L2}^2\right)}\left[\lambda_{L1}\left(\phi_{L1} - N_{L1}\right) - \lambda_{L2}\left(\phi_{L2} - N_{L2}\right)\right] \tag{10}$$

The carrier measurement of the ionospheric delay is significantly less noisy than the code measurement, but this measurement $I_{L1\phi}$ of the delay was offset from the correct absolute value because of the integer ambiguity. In Figure 4 the $I_{L1\phi}$ was re-centered using the time-averaged code measurement $I_{L1\rho}$. The green line is $I_{L1\rho\phi}$ given in equation (8).

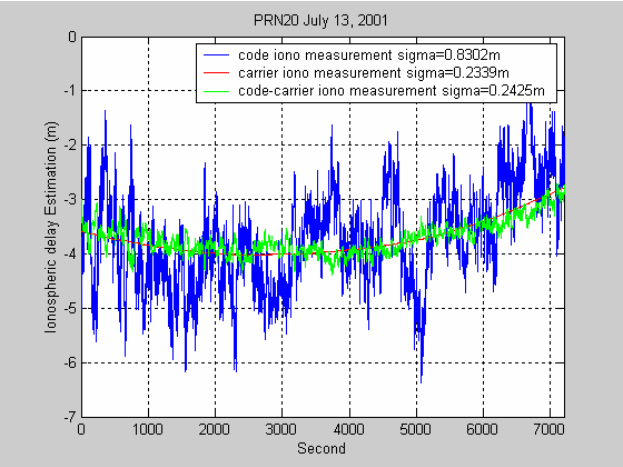

Figure 4: Slant ionospheric delay to satellite number 40 at Stanford University on July 13, 2001.

As shown in Figure 4, the code and carrier divergence technique provides good ionospheric delay estimation (the standard deviation $\sigma_{Code\_Carrier}$ is 0.2425m in this example), but cycle slips can not be tolerated. If cycle slips are present, the Phase Lock Loop (PLL) of GPS receiver will lose carrier tracking. Momentary loss of phase lock can result in a discontinuity in the integer cycle count. As a result, the integer ambiguity also has to be resolved.

For our precision approach example, when one aircraft loses L1 while descending into the RFI field, this aircraft can use the L5 code and carrier divergence technique to continue the ionospheric delay estimation. The nominal σ_{UIRE} will change as follow:

$$\begin{aligned} \sigma_{UIRE} &= \sigma_{UIRE\_L1L5} + \sigma_{Code\_Carrier} \\ &= 0.32 + 0.2425 \\ &\approx 0.56 \text{ (m)} \end{aligned} \tag{11}$$

The σ_{UIRE} in equation (11) is much less than the nominal σ_{UIRE_L5} using the WAAS grid which is of 6.0m. Based

on this model, users at SFO will be able to maintain good ionospheric delay estimation without using the WAAS grid for full duration of approach, provided cycle slips can be avoided. The SFO example is summarized in Figure 5.

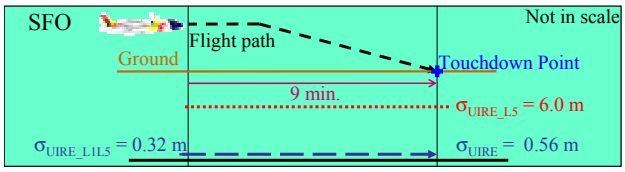

Figure 5: The nominal σ_{UIRE} variation along with the final approach in SFO. When the user lost L1 while descending into the RFI field, the user applies the L5 code and carrier divergence technique to continue to estimate the ionospheric delay instead of using the WAAS grid. This technique provides good ionospheric delay estimation for the full duration of the approach.

Figure 5 shows the simulation result for the typical precision approach example based on SFO. Next, we will use MAAST [4] to measure aircrafts applying this code carrier divergence technique at all airports within CONUS. The MAAST simulation configuration is specified in Table 1.

Table 1: The MAAST simulation Configuration.

Satellite Constellation	GEO	User	Time Step	VAL	HAL
24 standard GPS satellites (WAAS MOPS)	2 GEO's (AOR-W, POR)	1-degree user grid within CONUS	30-second over a 24-hour period	50 m	40 m

The MAAST is modified to adopt the changes in the UIRE calculation for an L1-L5 dual-frequency user losing L1 frequency while descending into the RFI field and then applying the L5 code and carrier divergence technique to continue the ionospheric delay estimation. The new UDRE calculation used in the MAAST simulation is given in equation (12). This σ_{UIRE} value may be aircraft specific.

$$\begin{aligned} \sigma_{UIRE} &= \sigma_{UIRE\_L1L5} + \sigma_{Code\_Carrier} \\ &= \sigma_{UIRE\_L1L5} + 0.2425 \text{ (m)} \end{aligned} \quad (12)$$

Figure 6 shows the simulation result, which is the 99.9% VPL contour for an L1-L5 dual-frequency user applying the code and carrier divergence technique to continue the ionospheric delay estimation while losing L1-frequency to RFI. Figure 6 shows the VPL values are less than 40m for 99.9% of time over 100% CONUS (Note: LPV VAL = 50m). Based on this simulation result, the L1-L5 dual-frequency aircraft while losing L1-frequency to RFI within CONUS will be able to use this technique to maintain good ionospheric delay estimation without using the WAAS grid for full duration of approach.

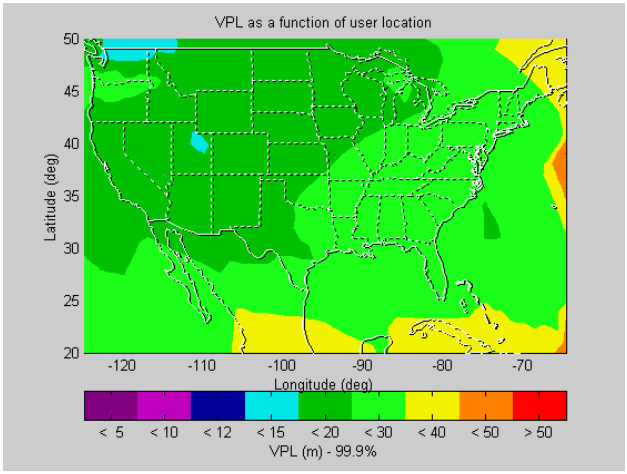

Figure 6: The 99.9% VPL contour for an L5 single-frequency user applying the code and carrier divergence technique to estimate the ionospheric delay after losing L1 frequency while descending into the RFI field.

In order to show the benefit for using the code and carrier divergence technique, the comparison of two VPL contours is shown in Figure 7. First, the VPL contour on the left is for an L1-L5 dual-frequency user using the code and carrier divergence technique to estimate the ionospheric delay after losing L1 frequency to the RFI. The VPL values in CONUS of this plot are greater than 12m but less than 40m. Second, the VPL contour on the right is for an L1-L5 user using the WAAS grid to estimate the ionospheric delay after losing L1 frequency to the RFI. The VPL values in CONUS of this plot are greater than 30m, and some places are higher than 50m (LPV VAL). Therefore, the VPL contour for using the code and carrier divergence technique is better than the VPL contour for using the WAAS grid. However, the cycle slip risk is accumulated. An L1-L5 dual-frequency user using the code and carrier divergence technique to estimate the ionospheric delay after losing L1 frequency to the RFI can have a performance similar to the L1-L5 dual-frequency user.

GPS receiver manufactures have their own algorithms to detect cycle slips. If there are cycle slips, the airborne user will no longer be able to use this technique and will have to use one of the other two techniques: the WAAS ionosphere threat model technique, and the maximum ionospheric delay gradient model technique.

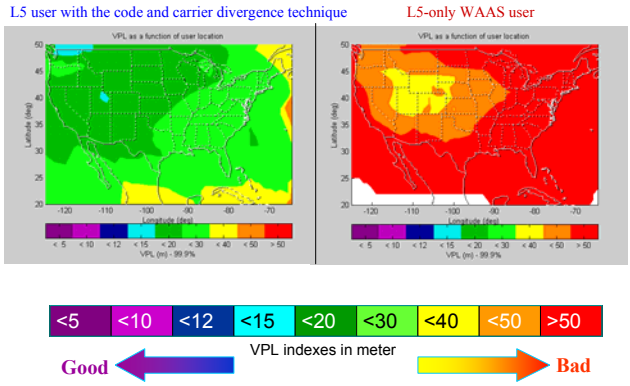

Figure 7: The comparison of the VPL contours. The VPL contour on the left is for an L1-L5 dual-frequency user using the code and carrier divergence technique to estimate the ionospheric delay after losing L1 frequency to the RFI. The VPL contour on the right is for an L1-L5 user using the WAAS grid to estimate the ionospheric delay after losing L1 frequency to the RFI. The color bar shows the VPL indexes in meters. The use of the code and carrier divergence technique provided better ionospheric delay estimation than using the WAAS grid for an L1-L5 dual-frequency airborne user descending into an L1 RFI field.

IV. THE WAAS IONOSPHERE THREAT MODEL TECHNIQUE

A future WAAS message could possibly include the new message bits to indicate the presence of an ionosphere storm in addition to the GIVE message. If there are cycle slips and the aircraft has such an ionosphere storm detector available, that aircraft can use the WAAS ionosphere threat model technique to bound the ionosphere error while descending into the RFI field.

This WAAS ionosphere threat model is detailed in [8]. That is a temporal threat model which models the deviations in time since the last planar fit. A plot of the temporal threat model is shown in Figure 8, which plots the histogram of equation (13).

$$\Delta I_{t=t_{iono}} = \hat{I}_{t=t_{iono}} - \hat{I}_{t=t_0} \qquad (13)$$

Where, $\hat{I}$ is the estimated ionospheric delay at a specific time.

In [8], only the points that pass the chi-square test are used in determining the threat model. The chi-square test is a reliable indicator of the "goodness of fit," and is used to detect the ionosphere irregularity. Readers can refer to [9] for more information about the chi-square test and the ionosphere irregularity detection.

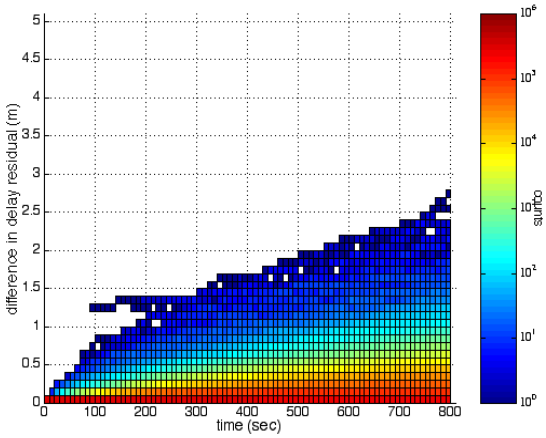

Figure 8: The temporal threat model. The maximum gradient occurs around 300 seconds which is 1.62m. (Courtesy: Lawrence Sparks)

Figure 9 shows the differences between fit residuals at the time of a fit and fit residuals at subsequent times. The gradient shows the ROT (Rate of TEC (i.e. Ionospheric delay)). In Figure 8 the maximum gradient occurs around 300 seconds which is 1.62m. The equation to overbound the *ROT* in Figure 8 is as follow:

$$ROT_{bound} = \begin{cases} 1.62\,\text{m, if t<120 sec} \\ \sqrt{1.62^2 + (5.33 * 0.00075 * (t-120))^2}\ \text{m, (14)} \\ \text{if t>120 sec} \end{cases}$$

The blue line in Figure 9 plots the ROT_{bound} and the red line in Figure 9 plots the confidence σ_{ROT}, which is calculated in equation (15).

$$\sigma_{ROT} = \begin{cases} \dfrac{1.62}{5.33}\ \text{(m), if t<120sec} \\ \dfrac{\sqrt{1.62^2 + (5.33 * 0.00075 * (t-120))^2}}{5.33}\ \text{(m), (15)} \\ \text{if t>120sec} \end{cases}$$

Where, 5.33 is K_{HMI} value defined in Appendix J of the WAAS MOPS [10], and 5.33 is used to convert a 10^{-7} error bound to one sigma level.

The overbound model is originally designed to protect the WAAS users using GIVE messages. As a result, this model is valid before the time receiving the next GIVE message, which is 600 seconds [8]. However, the blue line in Figure 9 still bounds the data shown in Figure 8 at 800 seconds.

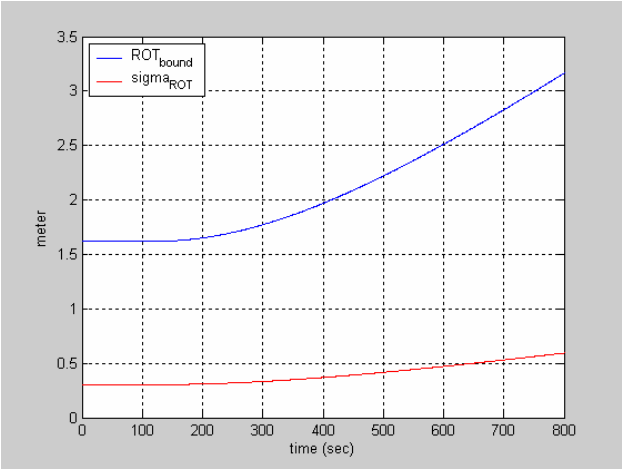

Figure 9: The WAAS ionosphere threat model (ROT overbound model). The blue line is ROT overbound model, and the red line represents the confidence of it.

For our precision approach example, when an aircraft lost L1 while descending into the RFI field, this aircraft can use the WAAS ionosphere threat model technique to bound the ionospheric error. The nominal σ_{UIRE} at the touchdown point can be calculated by substituting $t = 540$ sec into equation (15).

$$\sigma_{ROT_{bound}SFO} = \frac{\sqrt{1.62^2 + (5.33 * 0.00075 * (540 - 120))^2}}{5.33} = 0.4377 \text{ (m)} \quad (16)$$

$$\sigma_{UIRE} = \sigma_{UIRE\_L1L5} + \sigma_{ROT_{bound}SFO} = 0.32 + 0.4377 \approx 0.76 \text{ (m)} \quad (17)$$

The σ_{UIRE} in equation (17) is much less than the nominal σ_{UIRE_L5} = 6.0m for L5-only user. Based on this model, users at SFO will be able to maintain useful ionospheric delay estimation without using the WAAS grid for at least 10 minutes. The SFO example is summarized in Figure 10.

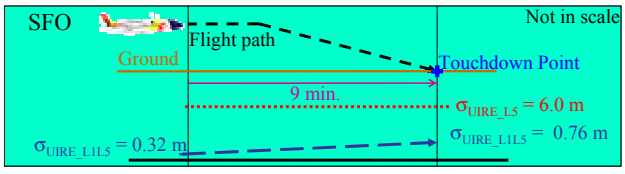

Figure 10: The nominal σ_{UIRE} variation along with the final approach in SFO. When user lost L1 while descending into the RFI field, user applies the WAAS ionosphere threat model technique to bound the ionospheric delay error and instead uses the WAAS grid. This technique provides good ionospheric delay estimation for at least 10 minutes.

Figure 10 shows the simulation result for the typical precision approach example based on SFO. Next, we will use MAAST to measure aircrafts applying this WAAS ionosphere threat model technique at all other airports within CONUS. The MAAST simulation configuration is specified in Table 1.

The MAAST is modified to adopt the changes in the UIRE calculation for an L1-L5 dual-frequency user losing L1 frequency while descending into the RFI field and then applying the WAAS ionosphere threat model technique to continue bound the ionosphere error.

This new UIRE calculation is a time dependent function; therefore, MAAST simulated the aircraft using the WAAS ionosphere threat model technique to bound the ionosphere error while 9-minute (at the touchdown point) after descending into the RFI field. The corresponding new UDRE calculations used in the MAAST simulation are given in equation (18), respectively.

$$\sigma_{UIRE} = \sigma_{UIRE\_L1L5} + \sigma_{ROT_{bound}\_9\min} = \sigma_{UIRE\_L1L5} + 0.4377 \text{ (m)} \quad (18)$$

Figure 11 shows the simulation result, which is the 99.9% VPL contour for an L1-L5 dual-frequency user applying the WAAS ionosphere threat model technique to bound the ionosphere error 9-minute after losing the L1-frequency to RFI. Figure 13 shows the VPL values are less than 40m for 99.9% of time over 100% CONUS (Note: LPV VAL = 50m). Based on this simulation result, the aircraft will be able to use this technique to bound the ionosphere error without using the WAAS grid 9-minute after entering the RFI field.

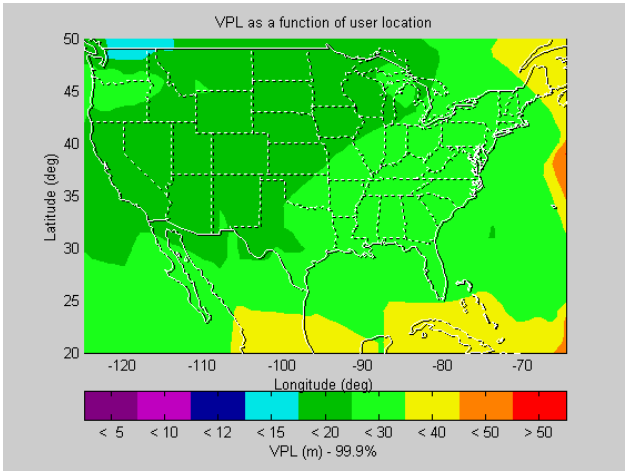

Figure 11: The 99.9% VPL contour for an L5 single-frequency user applying the WAAS ionosphere threat model technique to bound the ionosphere error after 9-minute descending into the RFI field (or at the touchdown point).

To show the benefit for using the WAAS ionosphere threat model technique, the comparison of two VPL contours is shown in Figure 12. First, the VPL contour on the left is for an L1-L5 dual-frequency user using the WAAS ionosphere threat model technique to bound the ionosphere error after losing L1 frequency to the RFI. The VPL values in CONUS of this plot are greater than 12m but less than 40m. Second, the VPL contour on the right is for an L1-L5 user using the WAAS grid to estimate the ionospheric delay after losing L1 frequency to the RFI. The VPL values in CONUS of this plot are greater than 30m, and some places are even greater than 50m (LPV VAL). Therefore, the VPL contour for using the WAAS ionosphere threat model technique is better than the VPL contour for using the WAAS grid. However, this technique requires an ionosphere storm detector. An L1-L5 dual-frequency user using the WAAS ionosphere threat model technique to estimate the ionospheric delay after losing L1 frequency to the RFI can have a performance similar to the L1-L5 dual-frequency user.

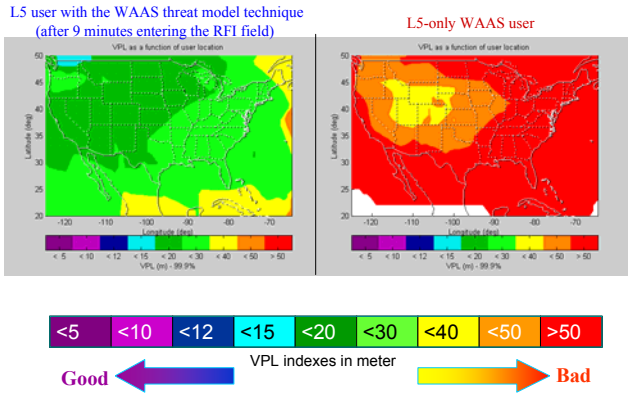

Figure 12: The comparison of the VPL contours. The VPL contour on the left is for an L1-L5 dual-frequency user using the WAAS ionosphere threat model technique to bound the ionosphere error after 9-minute losing L1 frequency to the RFI. The VPL contour on the right is for an L1-L5 user using the WAAS grid to estimate the ionospheric delay after losing L1 frequency to the RFI. The color bar shows the VPL indexes in meter. The use of the WAAS ionosphere threat model technique provided better ionospheric delay estimation than using the WAAS grid for an L1-L5 dual-frequency airborne user descending into an L1 RFI field.

The use of the WAAS ionosphere threat model technique requires an ionosphere storm detector. This ionosphere storm detector would need to listen to a new WAAS message which is designed to indicate the presence of an ionosphere storm. If there is an ionosphere storm or there is no available ionosphere storm detector, an aircraft will have to use the maximum ionospheric delay gradient model technique to sustain a performance similar to the dual-frequency ionospheric delay estimation while descending into the RFI field.

V. THE MAXIMUM IONOSPHERIC DELAY GRADIENT MODEL TECHNIQUE

If there may be cycle slips and there is no available ionosphere storm detector, that aircraft can use the maximum ionospheric delay model technique to bound the ionosphere error while descending into the RFI field. This maximum ionospheric delay gradient model is detailed in [11]. In her work, she analyzed the supertruth data, which is the ionosphere data obtained for the past few years for the CONUS region from the twenty-five WRS's. She found that the maximum ionospheric delay gradient is 6m/19km in vertical. In other words, the difference of the measured ionospheric vertical delay at location A and the measured ionospheric vertical delay at location B which is 19km apart from location A, could be 6m in the worst case, as shown in Figure 13. Thus, the confidence bound can be calculated as

$$\sigma_{MAX\_IONOgradient} = \left(\frac{6}{5.33}\right)\cdot\left(\frac{d}{19}\right) \qquad (19)$$

Where,

5.33 is K_{HMI} value defined in Appendix J of the WAAS MOPS

d is distance from the current position to the place with the last dual-frequency ionospheric delay estimation

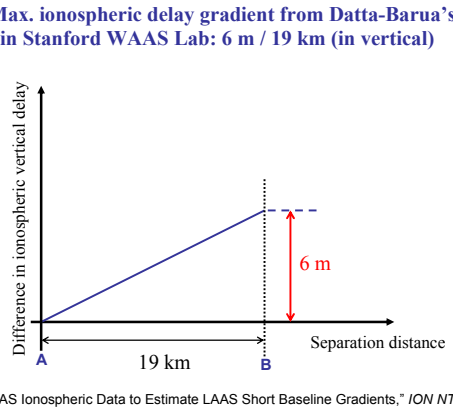

Figure 13: The maximum vertical ionospheric delay gradient model. The maximum difference in the ionospheric vertical delay for places 19 km apart ("A" and "B") is 6m [11].

If an aircraft loses L1 while descending into the RFI field, this aircraft can use the maximum ionospheric delay gradient model technique to bound the ionospheric error. The nominal σ_{UIRE} at the touchdown point can be calculated by substituting $d = 26.1$ km into equation (19).

$$\sigma_{MAX\_IONOgradientSFO} = \left(\frac{6}{5.33}\right)\cdot\left(\frac{26.1}{19}\right) = 1.5464 \text{ (m)} \quad (20)$$

$$\begin{aligned}\sigma_{UIRE} &= \sigma_{UIRE\_L1L5} + \sigma_{MAX\_IONOgradientSFO} \\ &= 0.32 + 1.5464 \\ &\approx 1.9 \text{ (m)}\end{aligned} \quad (21)$$

The σ_{UIRE} in equation (21) is much less than the nominal σ_{UIRE_L5} = 6.0m for L5-only user. Based on this model, users at SFO will be able to maintain useful ionospheric delay estimation without using the WAAS grid for at least 10 minutes. This SFO example is summarized in Figure 14.

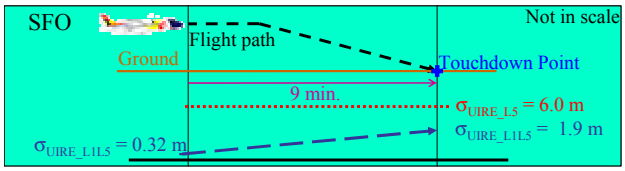

Figure 14: The nominal σ_{UIRE} variation along with the final approach in SFO. When the user lost L1 while descending into the RFI field, that user applies the maximum ionospheric delay gradient model technique to bound the ionospheric delay error and instead uses the WAAS grid. This technique provides good ionospheric delay estimation for at least 10 minutes of margin. The σ_{UIRE} at the touchdown point is 1.9m which is higher than the user with the WAAS ionosphere threat model in Figure 11.

Figure 14 shows the simulation result for the typical precision approach example based on SFO. Next, we will use MAAST to measure aircrafts applying this maximum ionospheric delay gradient model technique at all other airports within CONUS. The MAAST simulation configuration is specified in Table 1.

The MAAST is modified to adopt the changes in the UIRE calculation for an L1-L5 dual-frequency user losing L1 frequency while descending into the RFI field and then applying the maximum ionospheric delay gradient model technique to continue bound the ionosphere error. This new UIRE calculation is also a time dependent function; therefore, MAAST simulated the aircraft using the maximum ionospheric delay gradient model technique to bound the ionosphere error while 9-minute (at the touchdown point) after descending into the RFI field. The corresponding new UDRE calculations used in the MAAST simulation are given in equation (22).

$$\begin{aligned}\sigma_{UIRE} &= \sigma_{UIRE\_L1L5} + \sigma_{MAX\_IONOgradient9\min} \\ &= \sigma_{UIRE\_L1L5} + 1.5464 \text{ (m)}\end{aligned} \quad (22)$$

Figure 15 shows the simulation result, which is the 99.9% VPL contour for an L1-L5 dual-frequency user applying the maximum ionospheric delay gradient model technique to bound the ionosphere error 9-minute after losing the L1-frequency to RFI. Figure 15 shows the VPL values are less than 50m for 99.9% of time over 100% CONUS (Note: LPV VAL = 50m). Based on this simulation result, the L1-L5 dual-frequency aircraft while losing L1-frequency to RFI within CONUS will be able to use this technique to bound the ionosphere error without using the WAAS grid 9-minute after entering the RFI field.

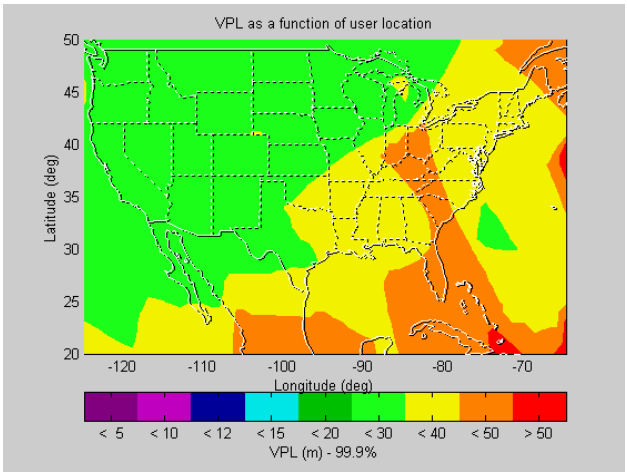

Figure 15: The 99.9% VPL contour for an L5 single-frequency user applying the maximum ionospheric delay gradient technique to estimate the ionospheric delay after 9-minute descending into the RFI field (or at the touchdown point).

To show the benefit for using the maximum ionospheric delay gradient model technique, the comparison of two VPL contours is shown in Figure 16. First, the VPL contour on the left is for an L1-L5 dual-frequency user using the maximum ionospheric delay gradient model technique to bound the ionosphere error after losing L1 frequency to the RFI. The VPL values in CONUS of this plot are greater than 20m but less than 50m. Second, the VPL contour on the right is for an L1-L5 user using the WAAS grid to estimate the ionospheric delay after losing L1 frequency to the RFI. The VPL values in CONUS of this plot are greater than 30m, and some places are even greater than 50m (LPV VAL). Therefore, the VPL contour for using the maximum ionospheric delay gradient model technique is better than the VPL contour for using the WAAS grid. An L1-L5 dual-frequency user using the maximum ionospheric delay gradient model technique to estimate the ionospheric delay after losing L1 frequency to the RFI can have a performance similar to the L1-L5 dual-frequency user.

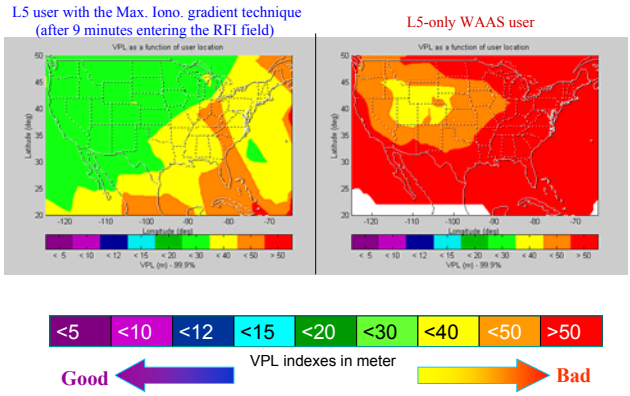

Figure 16: The comparison of the VPL contours. The VPL contour on the left is for an L1-L5 dual-frequency user using the maximum ionospheric delay gradient model technique to bound the ionosphere error 9-minute after losing the L1 frequency to the RFI. The VPL contour on the right is for an L1-L5 user using the WAAS grid to estimate the ionospheric delay after losing L1 frequency to the RFI. The color bar shows the VPL indexes in meter. The use of the maximum ionospheric delay gradient model technique provided better ionospheric delay estimation than using the WAAS grid for an L1-L5 dual-frequency airborne user descending into an L1 RFI field.

In summary, based on the information available to user, there are three techniques to sustain the dual-frequency ionospheric delay estimation. This analysis uses the typical precision approach example based on SFO to examine the possible solutions, and then use the MAAST to measure all airports over CONUS. First, one can use the code-carrier divergence technique to continue ionospheric delay estimation; this technique would require that there are no cycle slips. This technique provides good ionospheric delay estimation (better than using the WAAS grid) for the full duration of approach. Second, one can use the WAAS ionosphere threat model technique to bound the error. This technique requires an ionosphere storm detector. It provides useful ionospheric delay estimation for at least 10 minutes. Third, one can use the maximum ionospheric delay gradient model technique to estimate ionospheric delay during the ionosphere storm period. The maximum ionospheric delay gradient model technique also provides useful ionospheric delay estimation for at least 10 minutes. Figure 20 shows a summary comparison of the uses of these three techniques at the touchdown point. The VPL contour plots are shown in the order of the VPL performance from the left to the right. The use of the code and carrier divergence technique is the best, the use of the WAAS ionosphere threat model technique is the second, and the use of the maximum ionospheric delay gradient technique is the third. All of these techniques outperform the WAAS grid.

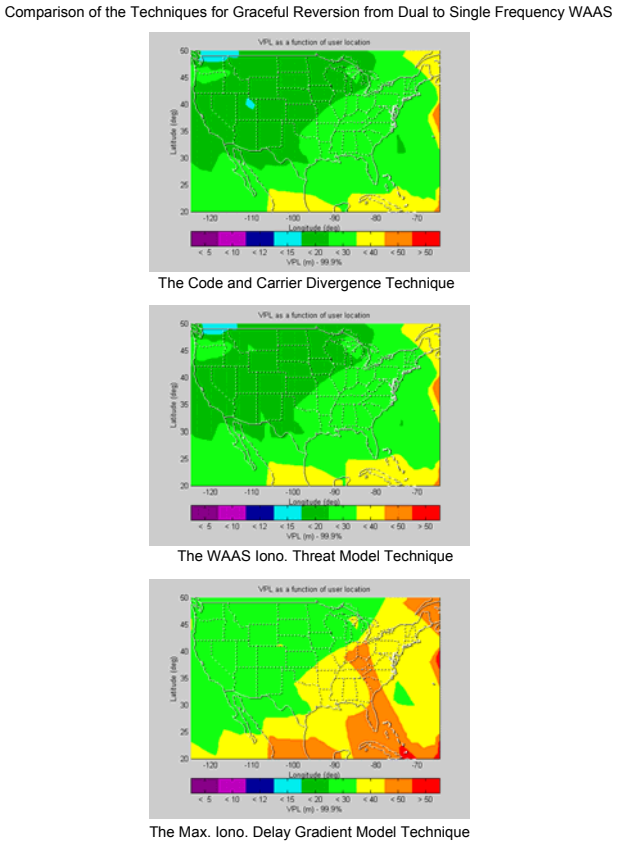

Figure 20: A summary comparison of the uses of these three techniques at the touchdown point. The VPL contour plots are shown in the order of the VPL performance from the left to the right. All of these techniques outperform the use of WAAS grid.

VII. CONCLUSIONS

This paper discussed the situation when an L1-L5 dual-frequency airborne user descended into the RFI field. This paper provided techniques for users to sustain a performance similar to the dual-frequency users. These techniques are the code and carrier divergence technique, the WAAS ionosphere threat model technique, and the maximum ionospheric delay gradient model technique. This paper first used a typical precision approach example based on San Francisco International Airport (SFO) to examine these techniques, and then used the MAAST to measure all airports over CONUS. The results are summarized in Table 2.

This paper demonstrated that a dual-frequency user can maintain the desired level of availability for LPV even when they lose all but one GPS frequency at the final approach fix point.

Table 2: The MAAST simulation results.

User Type	CONUS Coverage of APV 1.5 precision approach services (Availability ≥ 99.9%)	VPL (in meter)	HPL (in meter)
L1-L5 dual-frequency	100%	12 ≤ VPL < 40	5 ≤ HPL < 20
L1-only single-frequency	97.58%	20 ≤ VPL	15 ≤ HPL
L5-only single-frequency	49.25%	30 ≤ VPL	25 ≤ HPL
L5-only with the code and carrier divergence technique	100%	12 ≤ VPL < 40	5 ≤ HPL < 20
L5-only with the WAAS ionosphere threat model technique (after 9-minute losing L1)	100%	12 ≤ VPL < 40	5 ≤ HPL < 20
L5-only with the maximum ionospheric delay gradient model technique (after 9-minute losing L1)	100%	20 ≤ VPL < 50	10 ≤ HPL < 30

The 9-minute final approach duration used in this paper was derived from the final approach velocity of a general aviation (GA) aircraft, but these techniques are not limited to GA aircraft. The final approach velocities of the commercial airliner are faster than the GA aircraft, so the final approach duration is shorter in time. Therefore, these techniques will perform better on the commercial airliners than on the GA aircrafts.

ACKNOWLEDGEMENTS

The work in this paper is supported by the FAA Satellite Program Office under research grant 95-G-005. The authors gracefully acknowledge this support. The authors would also like to thank Dr. Demoz Gebre-Egziagher from University of Minnesota-Twin Cities for his thoughtful comments.

REFERENCES

[1] Navigation and Landing Transition Strategy, Federal Aviation Administration (FAA), Washington, D.C., August 2002.

[2] Jan, S.-S., Walter, T., Enge, P., "Analysis of a Three-Frequency GPS/WAAS Receiver to Land an Airplane," *Proceedings of ION GPS 2002*, Portland, OR, September 24-27, 2002.

[3] Jan, S.-S., Gebre-Egziabher, D., Walter, T. Enge, P., "Worst-Case Analysis of a 3-Frequency Receiver to Land a General Aviation Airplane," *Proceedings of ION NTM 2002*, San Diego, CA, January 28-30, 2002.

[4] Jan, S.-S., Chan, W., Walter, T., Enge, P., "MATLAB Simulation Toolset for SBAS Availability Analysis," *Proceedings of ION GPS 2001*, Salt Lake City, UT, September 11-14, 2001.

[5] Enge, P., Walter, T., Pullen, S., Kee, C., Chao, Y.-C., Tsai, Y.-J., "Wide Area Augmentation of the Global Positioning System," Proceedings of the IEEE, Volume: 84 Issue: 8, August, 1996.

[6] Misra, P., Enge, P., *Global Positioning System Signal, Measurements, and Performance*, Ganga-Jamuna Press, Lincoln, MA, 2001.

[7] Dai, D. H., Walter, T., Enge, P., Powell, J. D., "Optimal Use of Ionospheric Corrections for Wide Area Augmentation System (WAAS) Users," *IEEE Position Location and Navigation Symposium*, Rancho Mirage, CA, April 20-23, 1998.

[8] Sparks, L., Mannucci, A. J., Altshuler, E., Fries, R., Walter, T., Hansen, A., Blanch, J., Enge, P., "The WAAS Ionospheric Threat Model," *Beacon Satellite Symposium*, Boston, MA, 2001.

[9] Walter, T., Hansen, A., Blanch, J., Enge, P., Mannucci, T., Pi, X., Sparks, L., Iijima, B., El-Arini, B., Lejeune, R., Hagen, M., Altshuler, E., Fries, R., Chu, A., "Robust Detection of Ionospheric Irregularities," *Proceedings of ION GPS 2000*, Salt Lake City, UT, September 19-22, 2000.

[10] RTCA SC-159, *Minimum Operational Performance Standard for Global Positioning System/Wide Area Augmentation System Airborne Equipment*, RTCA/DO-229B, October 6, 1999.

[11] Datta-Barua, S., Walter, T., Pullen, S., Luo, M., Blanch, J., Enge, P., "Using WAAS Ionospheric Data to Estimate LAAS Short Baseline Gradients," *Proceedings of ION NTM 2001*, San Diego, CA, January 28-30, 2001.

[12] RTCA SC-159, *Minimum Aviation System Performance Standard for Local Area Augmentation Systems*, RTCA/DO-245, September 28, 1998.